Dehydration accelerates cytogenesis and cyst growth in Pkd1 −/− mice by regulating macrophage M2 polarization

Yang Yang (yybjzy@163.com)
The NO. 981 Hospital of Chinese People's Liberation Army
Minghui Song
Hainan Hospital of General Hospital of Chinese People's Liberation Army
Dongjuan Zhang
The NO. 981 Hospital of Chinese People's Liberation Army
Chao Wang
Beidaihe Rehabilitation and Recuperation Center of the Chinese People's Liberation Army
Jie Zhou
Shanghai University of Traditional Chinese Medicine
Lvjia Yi
Kidney Institution of the Chinese People's Liberation Army, Chang Zheng Hospital, the Navy Military Medical University
Meihan Chen
TongJi University
Changlin Mei
Kidney Institution of the Chinese People's Liberation Army, Chang Zheng Hospital, the Navy Military Medical University

Research Article

Keywords: adult autosomal dominant polycystic kidney disease, dehydration, macrophage, metabolism

Posted Date: December 20th, 2022

DOI: https://doi.org/10.21203/rs.3.rs-2379823/v1

Additional Declarations: No competing interests reported.

Version of Record: A version of this preprint was published at Inflammation on March 31st, 2023. See the published version at https://doi.org/10.1007/s10753-023-01806-5.

Abstract

Adult autosomal dominant polycystic kidney disease (ADPKD) has been shown to be related as a “third hit” to the occurrence of acute or chronic kidney injury. Here, we examined whether dehydration, as a common kidney risk factor, could cause cystogenesis in chronic-onset *Pkd*1$^{-/-}$ mice by regulating macrophage activation. First, we confirmed that dehydration accelerated cytogenesis in *Pkd*1$^{-/-}$ mice and that macrophages infiltrated the kidney tissues even earlier than macroscopic cyst formation. Then, microarray analysis suggested that glycolysis pathway may be involved in macrophage activation in *Pkd*1$^{-/-}$ kidneys under conditions of dehydration. Further, we confirmed glycolysis pathway was activated and lactic acid (L-LA) was overproduced in the *Pkd*1$^{-/-}$ kidney under conditions of dehydration. We have already proved that L-LA strongly stimulated M2 macrophage polarization and overproduction of polyamine in macrophage *in vitro*; and in the present study, we further discovered that M2 polarization-induced polyamine production shortened the primary cilia length by disrupting the PC1/PC2 complex. Finally, the activation of L-LA—arginase 1—polyamine pathway contributed to cystogenesis and progressive cyst growth in *Pkd*1$^{-/-}$ mice recurrently exposed to dehydration.

Introduction

Autosomal dominant polycystic kidney disease (ADPKD) is an inherited renal disease that is the fourth leading cause of renal replacement therapy (RRT) in the USA [1] and approximately 10% of end-stage renal disease (ESRD) in Europe [2]. ADPKD is not amenable to any specific treatment, necessitating only clinical management of its complications. The mechanisms underlying initial cystogenesis and later cyst growth in ADPKD have not been elucidated. Our previous study confirmed that M2-type macrophages promote cyst enlargement in the later stages of ADPKD in a rapid-onset polycystic kidney disease (PKD) mouse model, and showed that l-lactic acid (l-LA) acted as a key regulator influencing macrophage polarization in the polycystic kidney microenvironment.[3] Although we confirmed that macrophages play a vital role in the later phase of cyst enlargement (postnatal day [PD] 22–32), it is necessary to explore whether macrophages also affect initial cystogenesis (PD16–21) in the PKD mouse model. As the lifespan of rapid-onset PKD mice can be as short as PD35 and there is an unavoidable overlap between kidney development phase (before PD21) and the cystogenesis phase (PD16–21), it is understandable that the trigger of cystogenesis in the rapid-onset mouse model was kidney development. The limitations of the model were problematic for further exploration of the definite mechanism by which macrophages caused initial cystogenesis. To resolve this issue, we inactivated the *Pkd*1 gene in mice at PD30 to generate a chronic-onset mouse model. However, isolated microcysts were not detected until PD180 in this model. It has been reported that ischemia–reperfusion injury (IRI) could notably accelerate the development of PKD in a chronic-onset mouse model [4] and renal macrophages undergo a classical transition from M1 to M2 type [5]. However, IRI is not common in adult ADPKD, suggesting that other factors are involved in cystogenesis in adult ADPKD. Dehydration is a common cause of heat stress nephropathy, and severe dehydration may lead to acute kidney injury (AKI).[6] Non-severe or infrequent dehydration is often asymptomatic, but recurrent and severe dehydration may promote irreversible kidney injury and chronic

kidney dysfunction (chronic kidney disease [CKD]). Therefore, dehydration-induced kidney injury (DKI) can contribute to the AKI-to-CKD transition. Carlos et al. reported that DKI in wild-type mice resulted in the development of proximal tubular injury, macrophage infiltration, and kidney fibrosis, indicating that DKI is also likely to induce cystogenesis in mice with *Pkd*1 deficiency.[7] In the present study, we showed that DKI accelerated cystogenesis in a chronic-onset mouse model, thus providing an opportunity to comprehensively investigate the roles of macrophages in the development of ADPKD.

Materials And Methods

Establishment of chronic-onset PKD mice

We crossed C57/BL6 *Pkd1*$^{cond/cond}$ mice with C57/BL6 tamoxifen-Cre (B6. Cg-Tg [Cre/Esr1]) 5Amc/J mice (stock 004682; Jackson Laboratories) to produce the mice used in this study. To generate the chronic-onset PKD mouse model, we induced Cre recombinase activity in mice at P30 by intraperitoneal injection with tamoxifen (total dose: 300 mg/kg and 100 mg/kg on three sequential days) in coin oil. All experiments were performed using protocols approved by the Second Military Medical University Animal Care and Use Committee (SMMU-ACUC-20150430).

Animal Sample Collection

Mice were killed at the end of the dehydration period (that is, after the 7h dehydration protocol at 8 weeks) by anesthesia and cardiac exsanguination, and kidneys were processed for DNA and RNA extraction and histological examination (fixed in 4% paraformaldehyde buffered solution, pH 7.3–7.4). A sample of the kidney specimens was flash frozen in liquid nitrogen and immediately stored at − 80°C for further investigation.

Dehydration Protocol

The dehydration protocol consists of placing mice in a heated environment at 40°C for 30 min each hour for a total of 7h, 5 days a week, for a total duration of 8 weeks.

Microarray

The Agilent Sure Print G3 Mouse GE Microarray (8*60K, ID: 028005) was used. Total RNA was quantified with a Nano Drop ND-2000 (Thermo Scientific), and RNA integrity was assessed with an Agilent Bioanalyzer 2100 (Agilent Technologies). Sample labeling, microarray hybridization, and washing were performed according to the manufacturer's instructions. Briefly, total RNA was transcribed to double-strand complementary DNA (cDNA), synthesized into cRNA, and labeled with cyanine-3-CTP; the labeled cRNA was hybridized onto the microarray. After three washes, the arrays were scanned with the Agilent Scanner G2505C. Feature Extraction (version 10.7.1.1, Agilent Technologies) was used to analyze array

images to obtain raw data. Gene Spring (version 13.1, Agilent Technologies) was used to complete basic analyses of the raw data. The raw data were first normalized with the quantile algorithm. Probes with at least 100% of the values in any one of the conditions with flags in “detected” were chosen for further data analyses. Then we identified DEGs through fold changes. The threshold set for up- and downregulated genes was a fold change ≥ 2.0. Afterward, gene ontology and KEGG analyses were used to determine the roles of the differentially expressed mRNA.

Renal Function Evaluation

Plasma levels of creatinine were measured using a mouse creatinine assay kit (#80350, Crystal Chem, IL, USA).

Renal Tissue Analysis

An aliquot of each individual kidney sample or collected cells was precisely weighed and transferred to a microfuge tube. After adding 1 mL extraction solution (acetonitrile: methanol: water = 2: 2: 1), the samples were vortexed for 30 s, homogenized at 45 Hz for 4 min, and sonicated for 5 min in an ice-water bath. The homogenization and sonication steps were repeated three times, followed by incubation at −20°C for 1 h and centrifugation at 12,000 rpm and 4°C for 15 min. An 80 μL aliquot of the clear supernatant was transferred to an auto-sampler vial for liquid chromatography tandem mass spectrometry analyses. Stock solutions were prepared individually by dissolving or diluting each standard substance to a final concentration of 10 mmol/L. All standards were purchased from Sigma-Aldrich: pyruvic acid (107360), putrescine (51799), and mixed amino acid standards (A9906). A series of calibration standard solutions were prepared by stepwise dilution of this mixed standard solution with extraction solution. UHPLC separation was performed using an Agilent 1290 Infinity I Series UHPLC system (Agilent Technologies) equipped with a Water Acquity UPLC BEH Amide column (2.1 × 100 mm, 1.7 μm). An Agilent 6460 triple quadrupole mass spectrometer equipped with an AJS-ESI interface was used for assay development. The MRM parameters were optimized for each of the targeted analytes using flow injection analyses by injecting the standard solutions of the individual analytes into the API source of the mass spectrometer. At least two MRM transitions (i.e., the Q1/Q3 pairs) per analyte were obtained, and the two most sensitive transitions were used in the MRM scan mode to optimize the collision energy for each Q1/Q3 pair. Between the two MRM transitions per analyte, the Q1/Q3 pairs that showed the highest sensitivity and selectivity were used as the MRM transitions for quantitative monitoring. The additional transitions acted as qualifiers for verifying the identity of the target analytes. Agilent Mass Hunter Work Station (B.08.00) was used for MRM data acquisition and processing. The working standard solution was diluted in a stepwise manner with the extraction solution, with double dilution factors. Standard solutions were subjected to UHPLC-MRM-MS analyses. Signal-to-noise ratios were used to determine LLODs and LLOQs. LLODs and LLOQs were defined as the analyte concentrations that led to peaks with signal-to-noise ratios of 5 and 20, respectively. Kidney tissue (50 mg) was homogenized in 1 mL ice-cold 10% trichloroacetic acid (TCA) on ice. The same kidney tissue: TCA ratio

was used for all samples. Samples were centrifuged for 5 min at maximum speed. A 0.5 mL aliquot of the supernatant was transferred to a new microtube. Saturated ether (0.5 mL) was added to the supernatant, and the samples were vortexed for 20 s. The last two steps were repeated three times. Samples were left open in the fume hood for 30 min, and 50 µL each sample was mixed with 50 µL polyethylene glycol solution. The solution was mixed vigorously, incubated on ice for 30 min, and centrifuged at 13,000 rpm for 5 min at 4°C. The supernatant was transferred to a fresh tube and diluted five-fold with ice-cold dH2O prior to the assay. Then, an L-lactate (L-LA) assay kit (Cat#: A-108S and A-108L, Department of Biochemistry, University at Buffalo, Buffalo, NY, USA) was used to measure the levels of lactic acid in the kidney samples. The activity of pyruvate kinase and lactate dehydrogenase (LDH) in kidney samples were measured with colorimetric pyruvate kinase assay kit (#Ab83432) and colorimetric lactate dehydrogenase assay kit (#Ab102526).

Immunohistochemical Staining For Macrophage

Macrophage infiltration was assessed by immunostaining with a polyclonal anti-mouse monocyte–macrophage marker F4/80 diluted 1:50 (#ab111101). The number of positive cells for F4/80 was counted using an Image pro plus software (version 6.0). The software allows color recognition and positive cells were identified as % positive color saturation at 40×magnification in a blinded manner using at least 20 fields for each biopsy section. Macrophages highly expressing arginase 1 (ARG-1) were stained with monoclonal antibody against mouse ARG-1 diluted 1:50 (ab124917) and digital images were quantified at 40× magnification using Image pro plus software (version 6.0).

Cystic Index Calculation

Kidney sections (2 µm thick) were stained with hematoxylin and eosin (H&E) using routine procedures. Cyst formation was quantified from sagittal sections of whole kidneys. All specimens were scanned using Aperio XT, Leica Aperio (Leica Biosystems), and the raw data were read using Imagescope (version 12.3). The CI of whole kidney sections was calculated. Briefly, high-resolution whole kidney images were divided (along the longitudinal axis) into 20–30 small regions. Cystic areas in each split image and the whole kidney area were measured using Image Pro Plus (version 6.0) and the cystic areas were summed using Microsoft Excel 2010 as follows: CI of kidney specimen A = (Area of cysts in spit image 1 + 2 + 3 + 4…+n) / (Total area of kidney). cystic indices (CIs) were calculated from 5–6 kidney sections at each group and the mean CI was determined.

Identification Of Cell Proliferation In Kidney Sections

Ki-67 IHC staining was performed on paraffin sections (2 µm thick) of formalin-fixed tissue. All kidney sections were first incubated in 3% H2O2 followed by 4% serum from the host animal in which the relevant secondary antibody was generated. Then sections were incubated overnight at 4°C with primary antibodies against Ki-67 (#sc7844, 1:100, Santa Cruz Biotechnology; #ab15580, 1:100, Abcam). Signals

were detected using Dako EnVision Detection Systems Peroxidase/DAB kit, Rabbit/Mouse (#K5007) and VECTASTAIN® Elite® ABC-HRP kits (peroxidase, goat IgG, #PK-6105, CA, USA). Micrographs were randomly generated with a light microscope at 40× magnification. The numbers of positive and total nuclei were counted using Image Pro Plus (version 6.0). The ratio of Ki-67-positive nuclei to the total number of nuclei was calculated as a percentage using Microsoft Excel (version 2010). Images were captured from 5–6 kidney specimens at each postnatal age and 12–15 images were taken from each specimen (covering the cortex, C-M junction, and medulla).

Renal Macrophage Isolation And Sorting

Mouse kidneys were perfused through the left ventricle with ice-cold phosphate-buffered saline (PBS), excised, minced into small pieces (0.3–0.5 mm^3), and subjected to enzymatic digestion with a mixture of 500 U/mL collagenase I, 125 U/mL collagen XI, 60 U/mL DNase I, and 60 U/mL hyaluronidase for 1 hour at 37°C. The kidney tissues were triturated and filtered through a 40 μm nylon mesh. After erythrocyte lysis according to the manufacturer's instructions (1× RBC Lysis Buffer; eBioscience, San Diego, CA, USA), viable cells were resuspended in macrophage growth medium (DMEM/F12 containing 10% fetal bovine serum [FBS], 100 μM β-mercaptoethanol [#97622, Sigma], 5 μg/mL insulin, streptomycin—penicillin [1:1,000], and 10 μg/mL Fungin TM [#ant-fn-2; InvivoGen, San Diego, CA, USA]). Next, cells were split into Nunc™ EasY Flasks™ (75 cm^2; Thermo Scientific, Waltham, MA, USA) and cultured for 12 h at 37°C in an atmosphere of 95% air/5% CO_2. Adherent cells were detached using PBS supplemented with 5 mM EDTA. The harvested cells were washed twice in PBS and resuspended in FACS buffer (1% bovine serum albumin [BSA]/2 mM EDTA/PBS). Renal macrophages were purified as F4/80 (clone BM8)$^{+}$ CD11b (M1/70)^{high} by FACS. M1 and M2 macrophages were defined as Ly6C (clone HK1.4) ^{high} MR (clone C068C2) ^{low} and Ly6C ^{low} MR ^{high}, respectively.

Real-time Pcr

Total RNA was extracted using an RNase mini-kit (Invitrogen, Carlsbad, CA, USA) and reverse-transcribed. The primer sequences were detailed in the Supplementary materials. Real-time PCR was performed using SYBR Green PCR Master Mix (Toyobo, Osaka, Japan) and the Rotor-Gene 3000A real-time PCR system (Corbett, Sydney, Australia) according to the manufacturers' instructions. In brief, the PCR amplification reaction mixture (20 μL) contained 2 μL cDNA, 0.4 μL sense (F) primer, 0.4 μL anti-sense (R) primer, and 10 μL SYBR Green I. After initial denaturation at 95°C for 1 min, the reaction was cycled 45 times. Each cycle consisted of denaturation at 95°C for 15 s and primer annealing and extension at 60°C for 31 s. Results are shown as the relative expression of the targeted genes normalized to the expression of *Gapdh*. Real-time PCR was performed in triplicate for each experiment, and the average values were measured. Each experiment was repeated three times. Using the gene specific efficiencies, mRNA relative expression folds were calculated as $2^{-\Delta\Delta \text{ circle thresholdCT}}$.

Western Blot Analysis

Snap-frozen kidney tissue was homogenized in freshly prepared tissue protein extraction reagent (Pierce Bioscience, Rockford, IL, USA). Homogenates were centrifuged and the supernatants were stored at −80°C. Lysates in sodium dodecyl sulfate (SDS) sample buffer were boiled for 5 min at 95°C, and equal amounts of protein were resolved by SDS-polyacrylamide gel electrophoresis before transfer to a polyvinylidene difluoride membrane. The membrane was probed with primary antibody overnight at 4°C, followed by incubation with the secondary antibody for 2 h at room temperature. Proteins of interest were visualized by enhanced chemiluminescence. The average densitometry values of three independent experiments were measured. The primary antibodies were as follows: anti-LDHA (#ab52488, 1:1500, Abcam), anti-ARG1 (#ab124917, 1:2000, Abcam), anti-CD2-associated protein (CD2AP, #ab231320, 1:1000, Abcam), anti-PC2 (#ab244346, 1:2000, Abcam), and anti-GAPDH (#ab8245, 1:3000, Abcam).

Laser-scanning Confocal Imaging

For multiple fluorescence-IHC staining, deparaffinized kidney sections were incubated in 4% fetal bovine serum in phosphate-buffered saline (PBS) for 30 min followed by co-incubation with FITC-conjugated anti-F4/80 (#11–4801–82, 1:50, eBioscience, green) and anti-ARG1 (#ab124917, 1:50, Abcam) antibodies overnight at 4°C. Then, Alexa Fluor® 647-conjugated donkey anti-rabbit IgG (#ab150075, red) was applied as secondary antibody. Samples were mounted in Prolong® Gold Antifade with DAPI (blue) and visualized using a Leica TCS SP5 confocal scanning laser microscope (Leica Microsystems, IL, USA) and LAS AF Lite (version 2.6). Red, green, and blue images were merged using Image Pro Plus (version 6.0). Field images were taken with the 40–60× objective.

(2) In vitro experiments

Cell Culture

Human immortalized CLECs (OX-161) and RTECs (UCL-93) were kindly provided by Professor A.C. Ong (University of Sheffield, Sheffield, UK) and cultured as described previously (PMID: 26984954 DOI: 10.1152/ajprenal.00428.2015).

Immunofluorescence Microscopy

Immunofluorescence was carried out as previously described. Primary antibodies were used at the following dilutions: rabbit-origin antibody against PC2 (1:50), mouse-origin antibody against CD2AP (1:100, Clone: 5F8), rat-origin antibody against tubulin (1:200). Secondary antibodies used included Alexa Fluor® 488-conjugated goat anti-rabbit IgG (#ab150077, green), Alexa Fluor® 405-conjugated goat anti-mouse IgG (#ab175660, blue) and Alexa Fluor® 647-conjugated goat anti-rat IgG (#ab150167, red). Images were captured using a Leica TCS SP5 confocal scanning laser microscope (Leica Microsystems,

IL, USA) and LAS AF Lite (version 2.6). Red, green, and blue images were merged using Image Pro Plus (version 6.0).

Statistical analysis

All results are presented as mean ± SD. Variables were compared using Student's t-tests and Mann-Whitney U tests as appropriate. Data analyses were performed using SPSS (version 16.0), and $p < 0.05$ was considered to indicate significance.

Results

Dehydration promoted cyst growth in mice with Pkd1 gene deficiency

The *Pkd*1 gene was inactivated by tamoxifen at PD30 to generate a chronic-onset conditional knockout mouse model. Without any intervention, microcysts could be detected adjacent to the renal medulla–corticomedullary junction in PKD mice until PD180, and the cystic phenotype was severe at PD300 (Fig. 1A). However, cyst growth was more accelerated and progressive under conditions of dehydration. The dehydration protocol (Fig. 1B) resulted in varying degrees of sweating and weight loss in *Pkd*1$^{-/-}$ mice (Fig. 1C). Although the mice deprived of water during dehydration (water access at night [D-WAN]) would drink more water at night (Fig. 1D), they still showed significantly more weight loss compared with their *Pkd*1$^{-/-}$ littermates that had free access to water during dehydration (water at all times [D-WAT], Fig. 1E). Interestingly, although D-WAN and D-WAT mice drank approximately the same amounts of water during 24 hours (Fig. 1F), after 2 months of the intervention, cyst growth showed much greater progression in the D-WAN *Pkd*1$^{-/-}$ mice and their survival rates were significantly decreased compared with their D-WAT littermates (Fig. 1G—J).

Specific gene alteration in polycystic kidney during dehydration

Some genes were differentially expressed between the kidneys of D-WAT and control *Pkd*1$^{-/-}$ mice (Pool 1), D-WAN and control *Pkd*1$^{-/-}$ mice (Pool 2), and D-WAT and D-WAN *Pkd*1$^{-/-}$ mice (Pool 3, Fig. 2A). A total of 520 differentially expressed genes (DEGs) were common to Pools 1–3 (Fig. 2B). Microarray data have been deposited in the Array Express database at EMBL-EBI (www.ebi.ac.uk/arrayexpress) under the accession number E-MTAB-10449.

Cell location analysis based on the overlapping DEGs suggested that macrophages are key cells involved in the development of ADPKD in *Pkd*1$^{-/-}$ mice (Fig. 3A). Immunohistochemical staining confirmed that there were clusters of macrophages infiltrating around the interstitial tissues even before microcyst formation in the D-WAN *Pkd*1$^{-/-}$ mice (Supplementary Fig. 1). Gene Ontology (GO) enrichment analysis showed that macrophage polarization and activation were both associated with cyst growth after

dehydration in *Pkd*1$^{-/-}$ mice (Fig. 3B). Compared with D-WAT and control littermates, D-WAN *Pkd*1$^{-/-}$ kidney tissues exhibited strong activation of glycolysis, pyruvate metabolism, HIF-1 signaling pathway, and arginine-polyamine metabolism (Fig. 3C). Wiki pathway analysis further indicated that glycolysis pathway was possibly associated with macrophage polarization in D-WAN *Pkd*1$^{-/-}$ mice (Fig. 3D). By comprehensive bioinformatics analysis, we designated glycolysis pathway as the primary target to elaborate how dehydration facilitated cyst formation and development in *Pkd*1$^{-/-}$ mice via regulation of macrophage polarization **(Supplementary Figs. 2 and 3)**.

Glycolysis was activated in PKD mice when exposed to dehydration

Pyruvic acid and l-lactic acid (l-LA) were considered to be key metabolites during glycolysis **(Supplementary Fig. 4)**, and we showed that pyruvic acid and l-LA had already been overproduced in kidney tissues even before macroscopic cysts had formed in *Pkd*1$^{-/-}$ mice **(Supplementary Fig. 5)**, confirming that glycolysis was activated preceding organic renal hypoxia, which was due to cyst compression and vascular bed destruction (the Warburg effect). To investigate whether increased glucose intake promoted cyst development when exposed to recurrent dehydration, we gavaged *Pkd*1$^{-/-}$ mice with 25% glucose solution at 10 μl/g body weight (D-GLU group) via a plastic feeding tube (Instech Laboratories, Plymouth Meeting, PA, USA) under conditions of dehydration. Increased aerobic glycolysis is a prominent feature of the *Pkd*1$^{-/-}$ kidney and among the enzymes involved in glycolysis, lactate dehydrogenase (LDH) is emerging as an attractive target for possible pharmacological approaches in PKD therapy. We gavaged D-WAN mice with (R)-GNE-140 (D-GNE group), which is an effective LDH inhibitor, at a dose of 5 mg/kg/day. All groups had free access to water during the night (Fig. 4A). As expected, a marked decrease in survival rate accompanied progressive cyst enlargement and poorer renal function in the D-GLU group (Fig. 4B). Glucose intake significantly upregulated LDH protein expression, enhanced the activity of LDH, and produced more l-LA in polycystic kidneys **(Supplementary Fig. 6)**, resulting in marked stimulation of cyst lining epithelial cell (CLEC) proliferation and promotion of cyst growth in mice (Fig. 4C—H). As shown in Supplementary Fig. 6, the LDH activity and production of l-LA in polycystic kidneys were significantly inhibited after (R)-GNE-140 treatment, and the polycystic characteristics, renal function, and survival rates were notably improved in the D-GNE group despite identical glucose load to the D-GLU group. These observations strongly suggested that glycolysis and its final product, l-LA, play a vital role in dehydration-induced cyst enlargement in PKD mice.

Glycolysis-induced M2 polarization caused cytogenesis in Pkd1$^{-/-}$ mice

We have reported that l-LA could enhance the activity of arginase-1 (ARG1) and stimulate polyamine production in macrophages *in vitro* and confirmed that treatment with N-hydroxy-nor-l-arginine (nor-NOHA) markedly inhibited M2-macrophage polarization and postponed cyst development in chronic-onset *Pkd*1$^{-/-}$ mice.[3] In the present study, we showed that glucose intake under conditions of dehydration further stimulated the macrophage infiltrating polycystic kidneys (Fig. 5A). More than that, more

macrophages were driven toward the M2 type (Fig. 5B—F), and the expression of ARG1 were enhanced in these cells (Fig. 5G and H, and Supplementary Fig. 7). As a result, greater amounts of intermediate and final products of polyamine metabolism were produced in macrophages (Fig. 5I). By contrast, the renal characteristics described above in the D-GLU group were significantly reversed in the D-GEN group.

Polyamine shortened the cilia lengths on OX-161 cells by disrupting PC2-PC1 combination

Our previous work demonstrated that putrescine could stimulate the proliferation of fibroblasts and upregulate the expression of TGF-β both *in vivo* and *in vitro*. It would be helpful to determine the marked progression of renal fibrosis at the end stage of ADPKD. In the present study, we showed that putrescine also significantly shortened the primary cilia length of OX-161 cells, a human cyst-lining epithelial cell line (Fig. 6A and B). As shown in Supplementary Fig. 8, many proteins are associated with the expression of PC2 or PC1. *In vivo*, we compared the mRNA expression levels of these proteins between D-WAN and D-WAT polycystic kidney tissues, and found that CD2AP showed strongest upregulation in D-WAN *Pkd*1$^{-/-}$ kidney tissues (Fig. 6C). Putrescine at 1 mM significantly upregulated the expression of CD2AP and downregulated the expression of PC2 in OX-161 cells *in vitro* (Fig. 6D). Immunofluorescence analysis revealed that while endogenous PC2 localized to the plasma membrane and > 85% of the primary cilia in untreated OX-161 cells, those treated with putrescine showed striking loss of PC2 staining from these locations (~ 45%, Fig. 6E and F). Besides, the lengths of primary cilia on the PC2- OX-161 cells were significantly shorter than those on the PC2 + OX-161 cells when they were both treated with 1 mM putrescine for 16 h (Fig. 6G). For CD2AP dominantly expressed in the cytoplasm of OX-161 cells, the effect likely interrupted formation of the PC1/PC2 complex and disrupted the function of primary cilia (Fig. 7).

Discussion

This study was performed to elaborate the mechanism by which the microenvironment influences macrophage M2 polarization in polycystic kidney tissue under conditions of recurrent dehydration. Based on the results of bioinformatics analysis and our experience, we focused on the glycolysis–arginine–polyamine pathway, which caused macrophages to manifest M2 phenotype.

Recent studies have suggested that alternations in metabolic pathways may be critical in ADPKD and that defective glucose metabolism may be a hallmark offering new insight for investigating the roles of metabolic alterations in cystogenesis. Glucose is the main source of energy for the cell, and in the presence of oxygen, pyruvate is normally transported into mitochondria where it is converted into acetyl-CoA, which enters the tricarboxylic acid and is completely oxidized.[8] However, under hyperproliferative conditions, such as in early ADPKD, CLECs tend to show this inefficient process, even when oxygen is available. Rowe et al. suggested that cells lacking the *Pkd*1 gene tend to rely heavily on aerobic glycolysis as an energy source even when oxygen is available.[9] We also found that pyruvic acid and lactic acid were overproduced before massive cyst formation, confirming activation of glycolysis preceded hypoxia in

*Pkd*1$^{-/-}$ kidney tissues. Many animal and clinical studies have confirmed that interfering with glycolysis could have a beneficial effect on the progression of ADPKD. We confirmed that intake of fluid supplemented with glucose further enhanced the glycolysis burden in *Pkd*1$^{-/-}$ mice to produce more l-LA in kidney tissues. These observations indicate that sugared beverages could not replace water to supplement body fluid, especially for individuals with *Pkd*1 deficiency.

Our previous work indicated a role of the l-LA–arginine–polyamine pathway in the development of ADPKD.[3] As a cytokine, ARG1 could directly induce CLEC proliferation by the ERK–MRK pathway *in vitro*. As a key enzyme in regulation of arginine metabolism, activation of ARG1 resulted in overproduction of polyamines, including putrescine, spermidine, and spermine. Spermidine and spermine are intracellular molecules, while putrescine can diffuse into the cell membrane, and therefore putrescine is more likely to participate in intercellular interactions.[10] Putrescine has been shown to significantly stimulate TGF-β expression in fibroblasts.[11] It is reasonable to speculate that it plays an important role in renal fibrosis in the end stage of ADPKD in chronic-onset *Pkd*1$^{-/-}$ mice. With regard to the observation that putrescine shortened the lengths of primary cilia in CLECs, we focused more on the effects of polyamine on cilia function. In the adult kidney, primary cilia function as mechanosensors for luminal flow and play important roles in the control of cell proliferation.[12] There is accumulating evidence that primary cilia play key roles in normal physiological functions of RTECs, and that defects in ciliary function cause cytogenesis.[13 14] PC2 functions in a complex with PC1, and the present study included a number of experiments to examine the effects of polyamine on PC1-PC2 complex formation in renal epithelial cells. Among all proteins that may combine with PC1 or PC2, CD2AP showed the most significant upregulation in *Pkd*1$^{-/-}$ mice under conditions of dehydration. We found that putrescine elevated the expression of CD2AP by approximately 1.5-fold in CLECs, but not PC2, *in vitro*. CD2AP was named for its ability to bind CD2 and promote CD2 aggregation to stabilize the interaction between T cells and antigen-presenting cells.[15] It is ubiquitously expressed at higher levels in immune cells, epithelial cells, and neurons. Previous studies have shown that CD2AP is necessary for signaling at the slit diaphragm of the kidney.[16] It can combine with PC2 and disrupt PC1-PC2 combination to cause cystogenesis.[17]

This study had four limitations. First, the regulation of macrophage polarization is not limited to l-LA–arginine–polyamine pathway. Second, the composition of macrophage phenotypes in polycystic kidneys was not homogeneous and would change at different stages of ADPKD. Third, the elements regulating macrophage M2 polarization were not isolated but were closely interconnected with one another. In addition, macrophage polarization was likely to change according to alterations in protein expression. Finally, alteration of the microenvironment did not unbalance macrophage polarization, but rather caused macrophages to achieve a new equilibrium to better adapt to the altered homeostasis. It may be necessary to maintain the stability of homeostasis, but at the whole-body level it likely further drove progression of the disease.

Declarations

Competing interests: none.

Declarations of interest: none.

Availability of data and materials: Microarray data have been deposited in the Array Express database at EMBL-EBI (www.ebi.ac.uk/arrayexpress) under the accession number E-MTAB-10449.

Author contributions

Yang Yang and Changlin Mei designed the study; Yang Yang, Minghui Song, Chao Wang, Dan Zhou, Jie Zhou, Jiayi Lv, Shuwei Song, and Meihan Chen carried out experiments; Dongjuan Zhang analyzed the data; Dongjuan Zhang made the figures; Yang Yang drafted the paper; all authors approved the final version of the manuscript.

Acknowledgments

The present work was supported by the following grants: (1) The National Natural Science Foundation of China (81700579, 81670612); (2) The Three-year Project of Action for Shanghai Public Health System (GWIV—18); (3) The National Key Research and Development Program of China (2016YFC0901502); (4) Shanghai Top Priority Key Clinical Disciplines Construction Project (2017ZZ02009); and (5) the 13th Five-Year Key Plan for the Military Medical Scientific Research Project (CBJ14L016). No authors have any financial conflicts of interest.

References

1. Ong AC, Devuyst O, Knebelmann B, Walz G. (2015) Autosomal dominant polycystic kidney disease: the changing face of clinical management. *Lancet*.385:1993-2002. doi: 10.1016/s0140-6736(15)60907-2
2. Spithoven EM, Kramer A, Meijer E, Orskov B, Wanner C, Abad JM, Aresté N, de la Torre RA, Caskey F, Couchoud C, et al. (2014) Renal replacement therapy for autosomal dominant polycystic kidney disease (ADPKD) in Europe: prevalence and survival--an analysis of data from the ERA-EDTA Registry. *Nephrol Dial Transplant*.29 Suppl 4:iv15-25. doi: 10.1093/ndt/gfu017
3. Yang Y, Chen M, Zhou J, Lv J, Song S, Fu L, Chen J, Yang M, Mei C. (2018) Interactions between Macrophages and Cyst-Lining Epithelial Cells Promote Kidney Cyst Growth in Pkd1-Deficient Mice. *J Am Soc Nephrol*.29:2310-2325. doi: 10.1681/asn.2018010074
4. Takakura A, Contrino L, Zhou X, Bonventre JV, Sun Y, Humphreys BD, Zhou J. (2009) Renal injury is a third hit promoting rapid development of adult polycystic kidney disease. *Hum Mol Genet*.18:2523-2531. doi: 10.1093/hmg/ddp147
5. Belliere J, Casemayou A, Ducasse L, Zakaroff-Girard A, Martins F, Iacovoni JS, Guilbeau-Frugier C, Buffin-Meyer B, Pipy B, Chauveau D, et al. (2015) Specific macrophage subtypes influence the

progression of rhabdomyolysis-induced kidney injury. *J Am Soc Nephrol*.26:1363-1377. doi: 10.1681/asn.2014040320

6. Wesseling C, Aragón A, González M, Weiss I, Glaser J, Rivard CJ, Roncal-Jiménez C, Correa-Rotter R, Johnson RJ. (2016) Heat stress, hydration and uric acid: a cross-sectional study in workers of three occupations in a hotspot of Mesoamerican nephropathy in Nicaragua. *BMJ Open*.6:e011034. doi: 10.1136/bmjopen-2016-011034
7. Roncal Jimenez CA, Ishimoto T, Lanaspa MA, Rivard CJ, Nakagawa T, Ejaz AA, Cicerchi C, Inaba S, Le M, Miyazaki M, et al. (2014) Fructokinase activity mediates dehydration-induced renal injury. *Kidney Int*.86:294-302. doi: 10.1038/ki.2013.492
8. Gray LR, Tompkins SC, Taylor EB. (2014) Regulation of pyruvate metabolism and human disease. *Cell Mol Life Sci*.71:2577-2604. doi: 10.1007/s00018-013-1539-2
9. Rowe I, Chiaravalli M, Mannella V, Ulisse V, Quilici G, Pema M, Song XW, Xu H, Mari S, Qian F, et al. (2013) Defective glucose metabolism in polycystic kidney disease identifies a new therapeutic strategy. *Nat Med*.19:488-493. doi: 10.1038/nm.3092
10. Rojas-Martínez C, Rodríguez-Vivas RI, Figueroa Millán JV, Acosta Viana KY, Gutiérrez Ruiz EJ, Álvarez Martínez JA. (2017) Putrescine: Essential factor for in vitro proliferation of Babesia bovis. *Exp Parasitol*.175:79-84. doi: 10.1016/j.exppara.2017.01.010
11. Yang Y, Ma L, Song M, Li X, He F, Wang C, Chen M, Zhou J, Mei C. (2020) The role of the complement factor B-arginase-polyamine molecular axis in uremia-induced cardiac remodeling in mice. *Eur J Immunol*.50:220-233. doi: 10.1002/eji.201948227
12. Wang S, Dong Z. (2013) Primary cilia and kidney injury: current research status and future perspectives. *Am J Physiol Renal Physiol*.305:F1085-1098. doi: 10.1152/ajprenal.00399.2013
13. Cantagrel V, Silhavy JL, Bielas SL, Swistun D, Marsh SE, Bertrand JY, Audollent S, Attié-Bitach T, Holden KR, Dobyns WB, et al. (2008) Mutations in the cilia gene ARL13B lead to the classical form of Joubert syndrome. *Am J Hum Genet*.83:170-179. doi: 10.1016/j.ajhg.2008.06.023
14. Duldulao NA, Lee S, Sun Z. (2009) Cilia localization is essential for in vivo functions of the Joubert syndrome protein Arl13b/Scorpion. *Development*.136:4033-4042. doi: 10.1242/dev.036350
15. Dustin ML, Olszowy MW, Holdorf AD, Li J, Bromley S, Desai N, Widder P, Rosenberger F, van der Merwe PA, Allen PM, et al. (1998) A novel adaptor protein orchestrates receptor patterning and cytoskeletal polarity in T-cell contacts. *Cell*.94:667-677. doi: 10.1016/s0092-8674(00)81608-6
16. Tolvanen TA, Dash SN, Polianskyte-Prause Z, Dumont V, Lehtonen S. (2015) Lack of CD2AP disrupts Glut4 trafficking and attenuates glucose uptake in podocytes. *J Cell Sci*.128:4588-4600. doi: 10.1242/jcs.175075
17. Sever S, Reiser J. (2015) CD2AP, dendrin, and cathepsin L in the kidney. *Am J Pathol*.185:3129-3130. doi: 10.1016/j.ajpath.2015.06.022

Figures

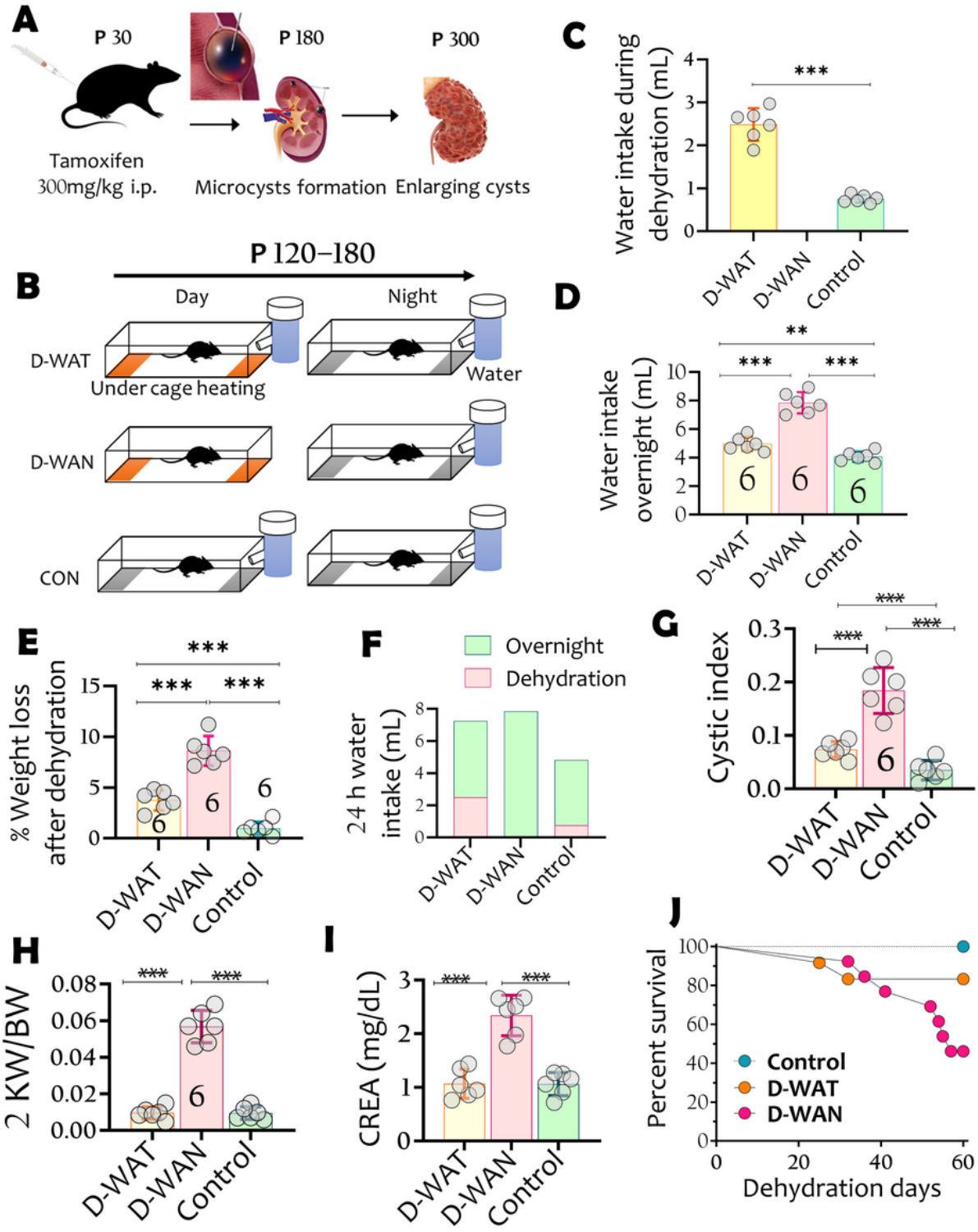

Figure 1

Dehydration altered the gene expression in polycystic kidney

(A) The generation of chronic-onset PKD mouse model. The mice were intraperitoneally injected with tamoxifen (TAM) at 300 mg/kg at the postnatal day 30 (PD 30) and isolated micro cyst cannot be detected around the medulla–corticomedullary junction until PD 180. (B) The dehydration protocol

consists of placing mice in a heated environment at 40 OC for 30min each hour for a total of 7h, 5 days a week, for a total duration of 8 weeks. Mice were divided into three groups. Mice in the first group received daily dehydration but with water provided during the periods between the heat exposure (D-WAT). Mice in the second group were dehydrated but provided water only for 12 h each night (D-WAN). Mice in the third group consisted of mice that were never dehydrated and water was provided ad libitum (control). (C) Water intake during dehydration. (D) Percent weight loss after 7-hour dehydration. (E) Water intake overnight. (F) 24-hour water intake. Dehydration notably accelerated cyst formation and developed cyst enlargement in PKD kidneys; G, cystic indices; H, two kidney weight/ body weight ratio. As a result, renal dysfunction (I) and survival rate (J) was deteriorated in the D-WAN group. The average value of one group was achieved from six independent mice. Data are mean ± SD; one-way ANOVA.

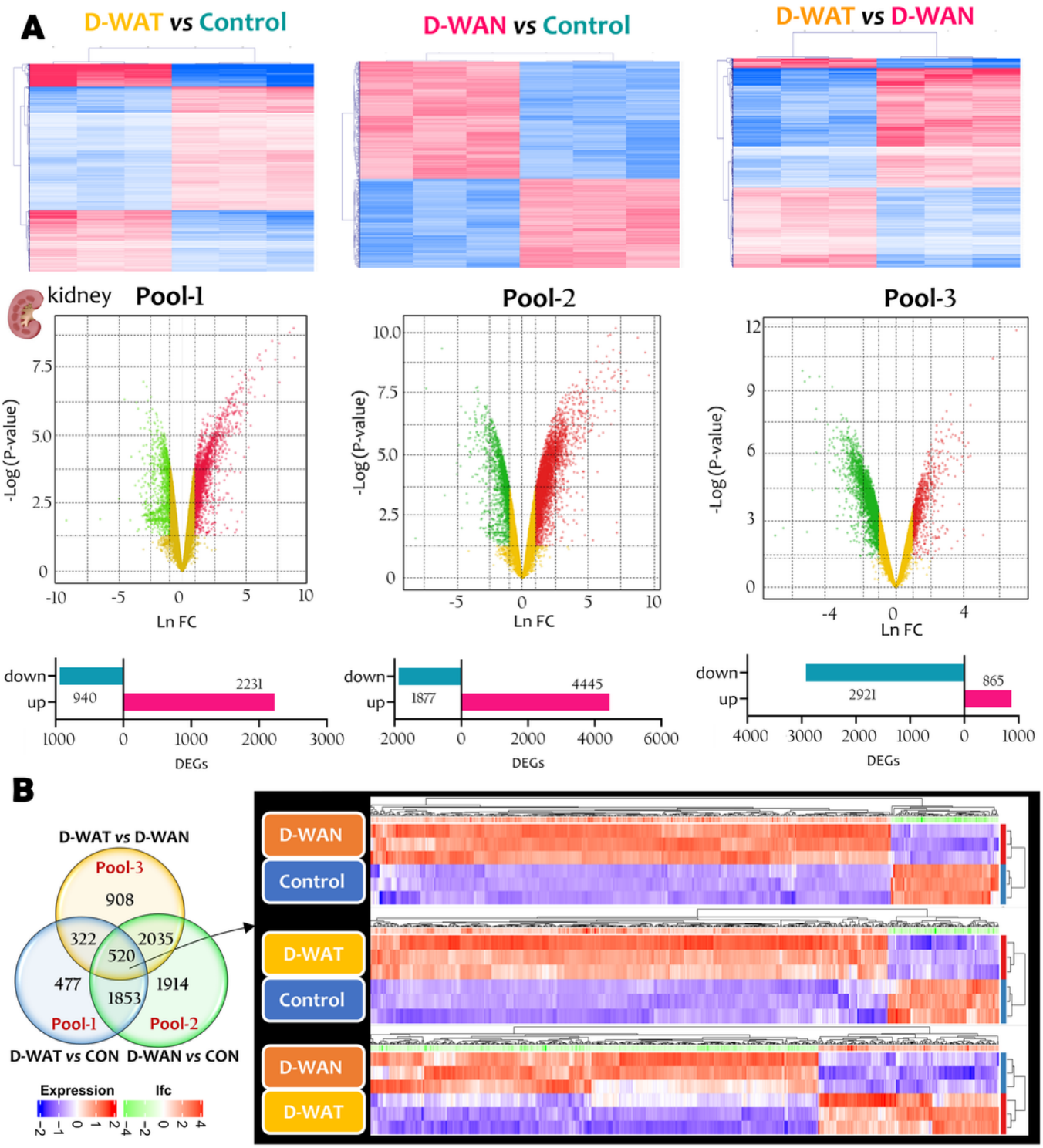

Figure 2

Special gene expression in polycystic kidneys after recurrent dehydration

(A) Heat maps. Some genes were differentially expressed between the kidneys of D-WAT and control mice with Pkd1 gene deficiency (Pool 1), D-WAN and D-WAT mice with Pkd1 gene deficiency (Pool 2), and D-WAN and control mice with Pkd1 gene deficiency (Pool 3). Upregulated (red) and downregulated (green)

differentially expressed genes (DEGs) in pool1, 2 and 3. The microarray data was achieved from independent three mice in one group. Data are mean ± SD; one-way ANOVA. (B) In total, 520 DEGs were common to Pools–3.

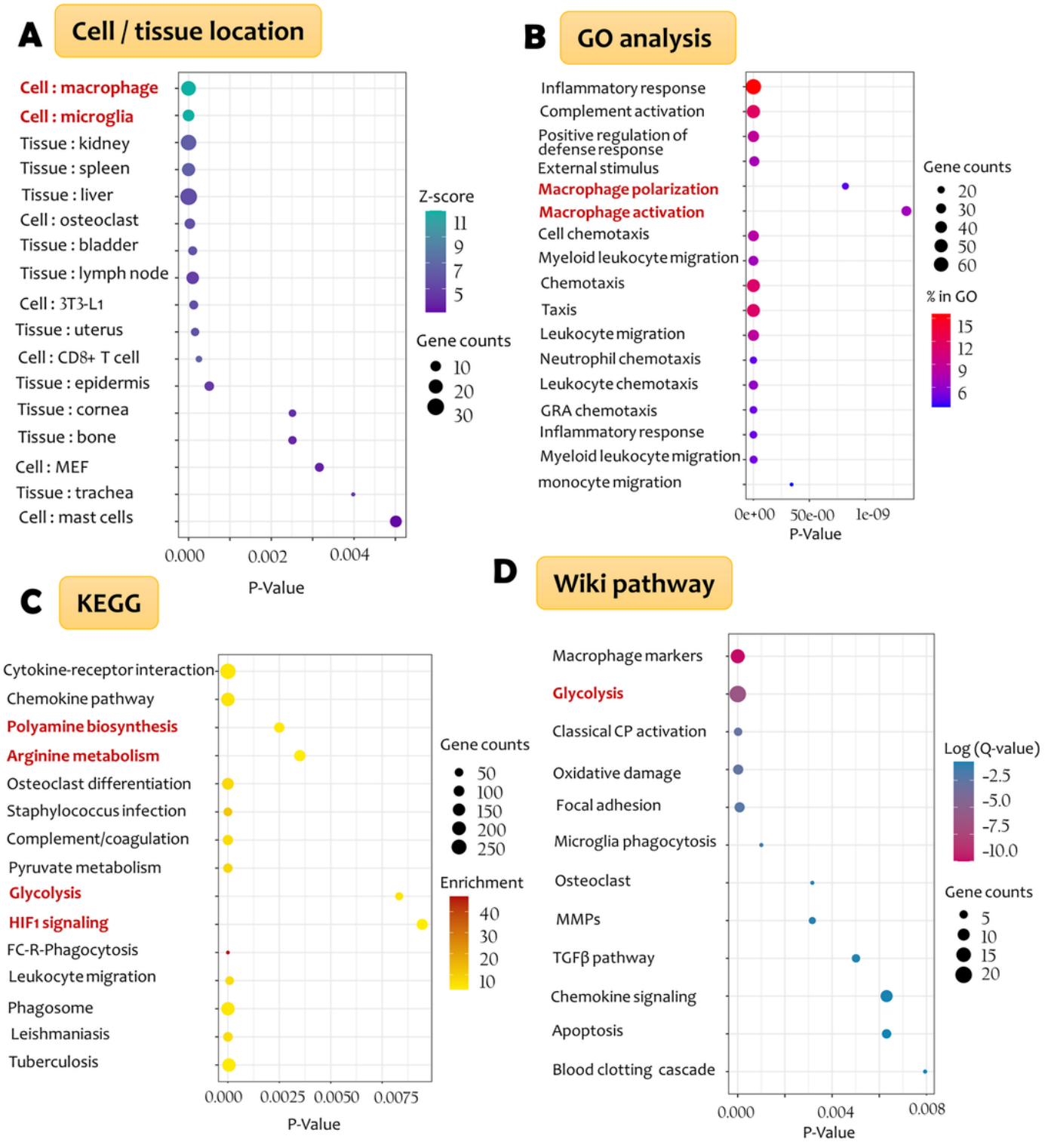

Figure 3

Signaling analysis based on microarray

(A) Cell/tissue specific analysis, (B) Gene Ontology (GO), (C) Kyoto Encyclopedia of Genes and Genomes (KEGG) and (D) Wiki pathway analyses for the common DEGs.

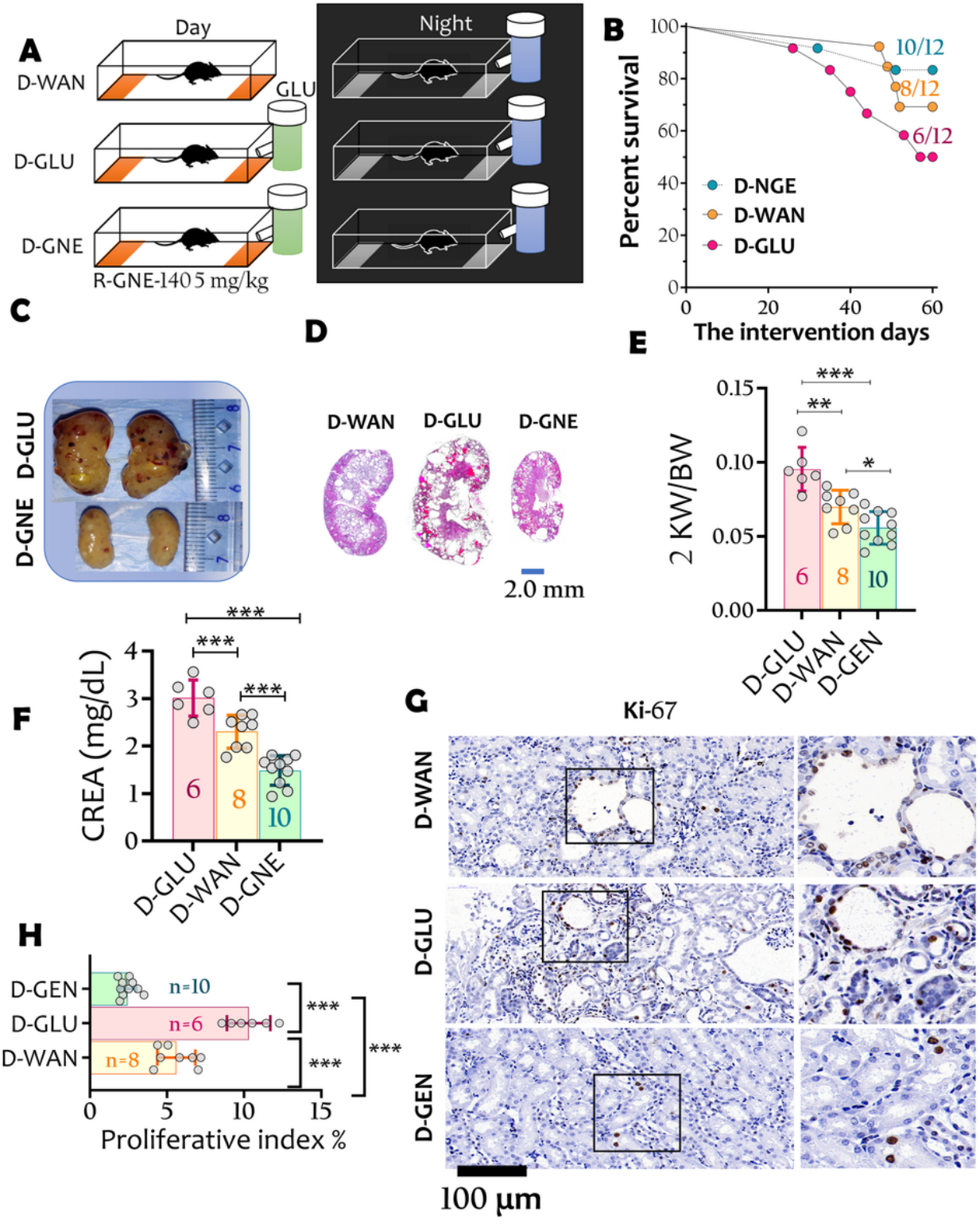

Figure 4

Glycolysis was activated in polycystic kidneys after recurrent dehydration

(A) The mice in one group received D-WAN procedure. The mice in another group were fed by 25% glucose (10 μL/g) during dehydration (D-GLU). The mice in third group were fed by 25% glucose and LHD inhibitor R-GNE-140 at 5 mg/kg/day during dehydration (D-GNE). (B) Survival rates among D-WAN, D-GLU and D-GNE groups. (C, D) Gross appearance of kidneys in D-WAN, D-GLU and D-GNE groups, respectively. (E, F) Two kidney weights/ body weight (2KW/BW) ratios (E) and serum creatinine levels (F) were compared among D-WAN, D-GLU and D-GNE groups. (G, H) Renal cell proliferation was evaluated using Ki-67 IHC staining. The average value of one group was achieved from six independent mice. Data are mean ± SD; one-way ANOVA.

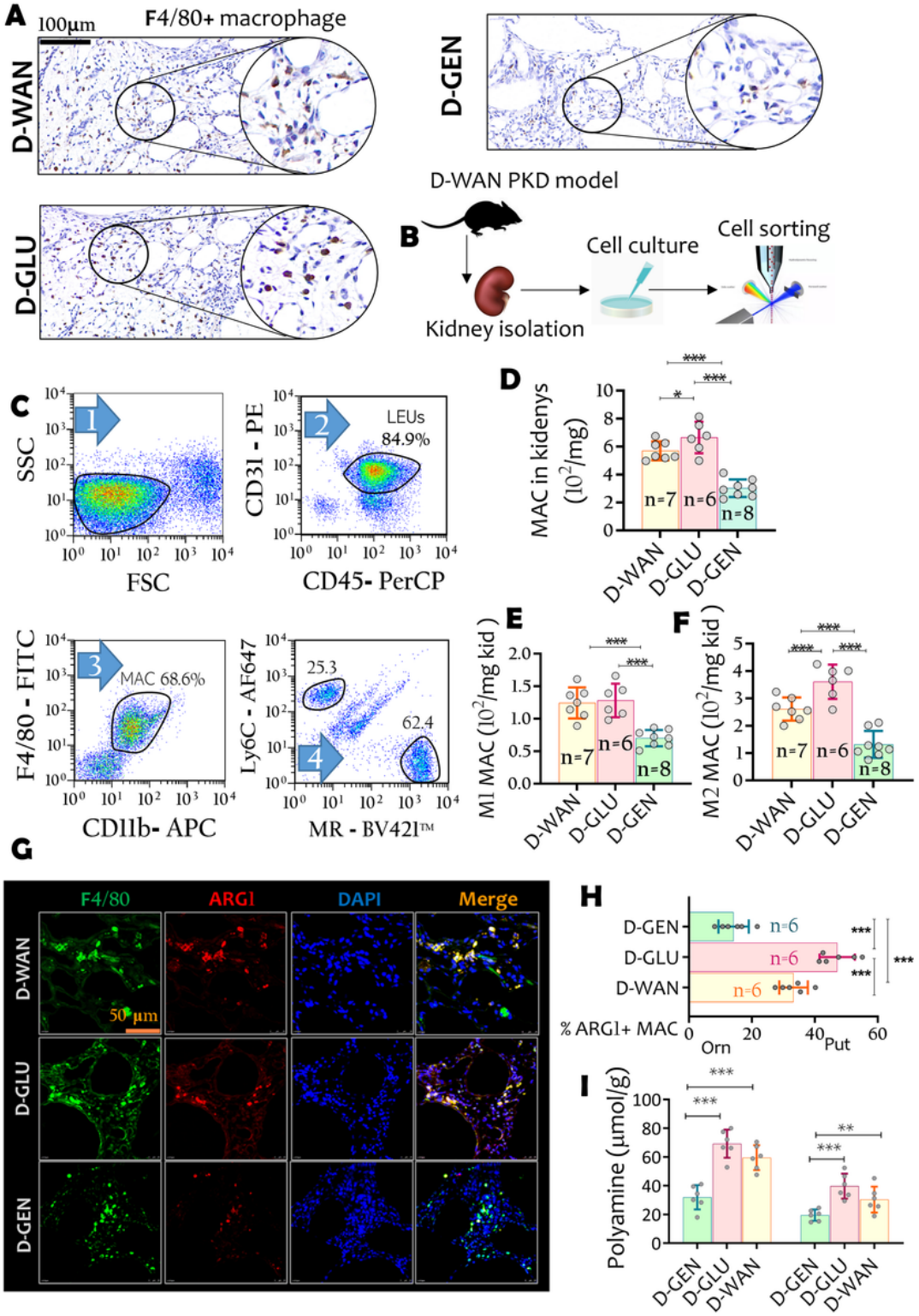

Figure 5

L-LA-induced M2 polarization and polyamine production in macrophage

(A) Renal macrophages infiltrating polycystic kidneys were labeled using F4/80 IHC staining. (B, C) Macrophages were isolated from kidneys using Fluorescence-activated cell sorting (FACS). (D–F) The general (D), M1- (E) and M2-type (F) macrophage counts in polycystic kidneys were compared among

different groups. (G, H) Triple-channel immunofluorescent staining to label ARG1 positive macrophages in kidneys. Green, F4/80; red, ARG1; and bule, DAPI (nuclei). (I) The levels of ornithine and putrescine in renal macrophages were measured using the NMR-based metabonomic method. The average value of one group was achieved from six independent mice. Data are mean ± SD; one-way ANOVA.

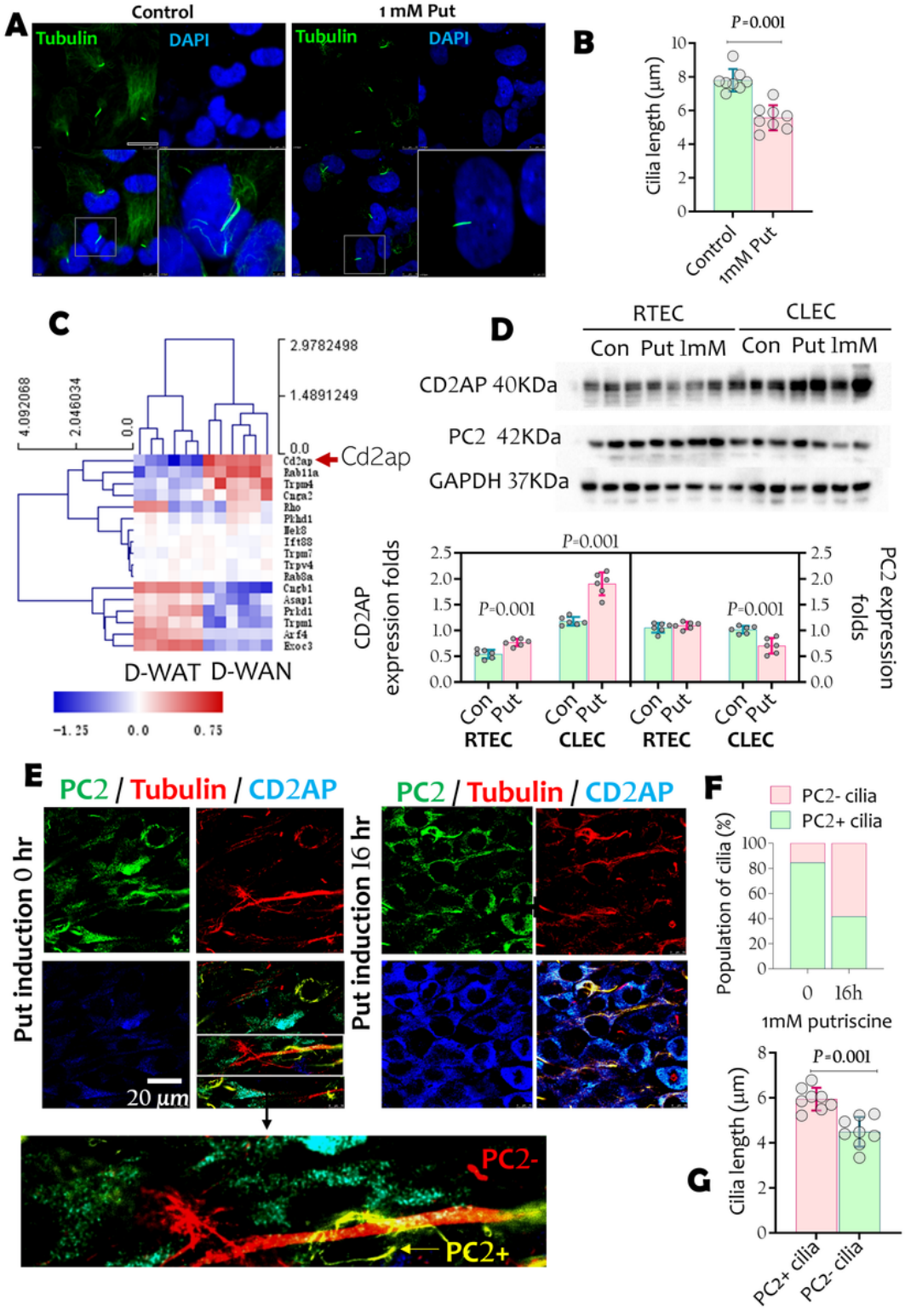

Figure 6

Putrescine shorten primary cilia by disrupting PC2/PC1 combination

(A, B) Putrescine at 1 mM significantly shortened the length of primary cilia on human cyst-lining epithelial cells (OX-161 cells). (C) The expression of CD2AP was significantly more enhanced in the kidneys of D-WAN *Pkd*1$^{-/-}$ mice, compared with those in the D-WAT counterparts. (D) Western blot analysis shows increased CD2AP protein levels but not PC2 protein levels in human cyst-lining epithelial cell line (CLECs, OX-161) upon putrescine at 1mM stimulation for 16 hours. Human RTEC cell line is UCL-93. (E, F) Triple immunofluorescence staining of endogenous PC2 (green), acetylated tubulin (red) and CD2AP (blue) in OX-161 cell line before or after stimulation with 1mM putrescine for 16 hours, observed with confocal microscopy. PC2 highly expressed in the yellow primary cilia while not expressed in the red primary cilia. The Figure shows that putrescine significantly decreased the percentage of primary cilia that highly expressed PC2 on OX-161 cell line. (G) The cilia lengths on OX-161 on PC2- and PC2+ OX-161 cells when treated with 1 mM putrescine for 16 hours, respectively. The average value of one group was achieved from six-eight independent cell specimens. Data are mean ± SD; t-test.

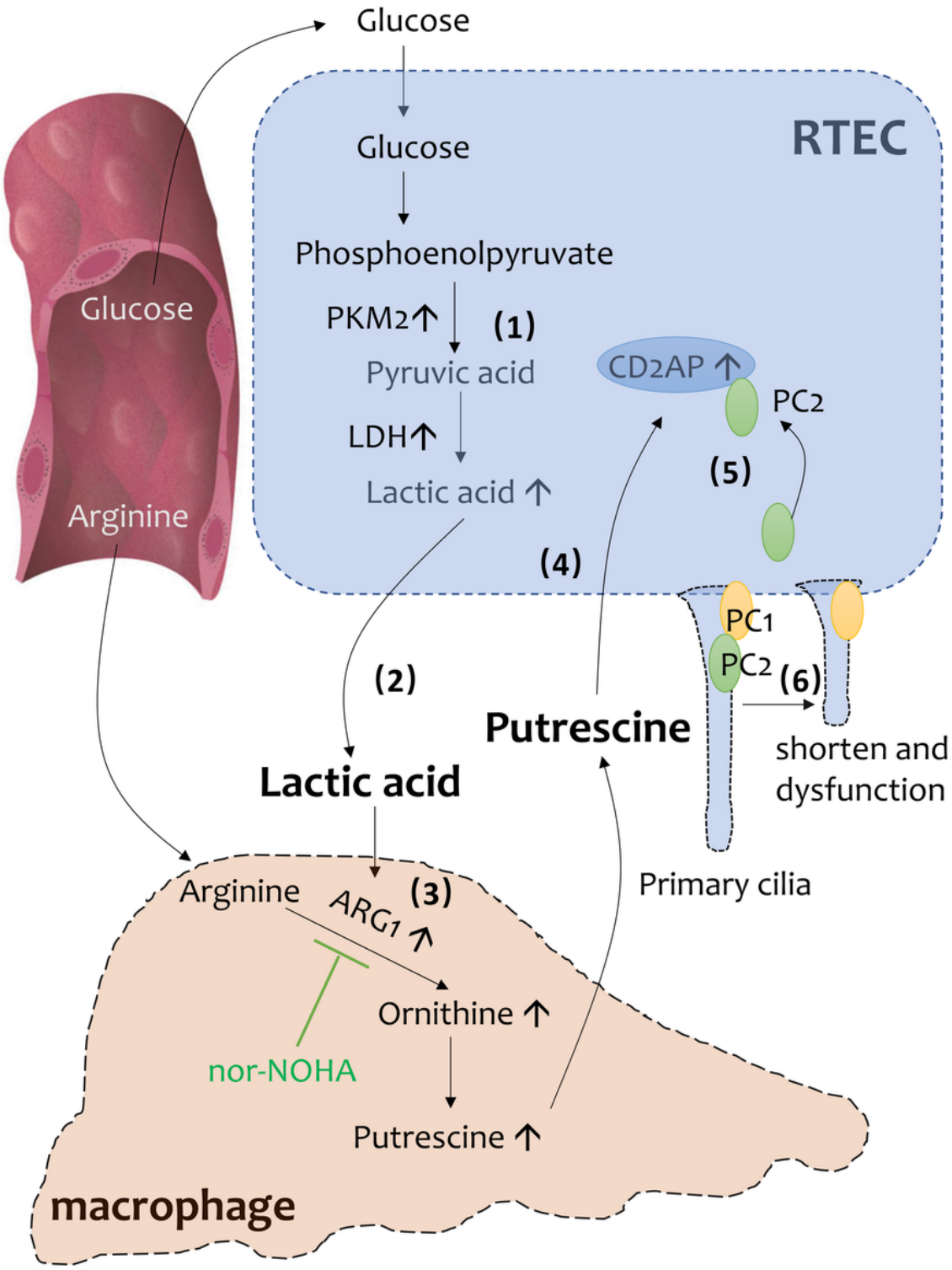

Figure 7

L-LA–putrescine–CD2AP axis promoted cytogenesis in Pkd1-/- mice when they were exposed to recurrent dehydration.

(1) RTECs lacking the Pkd1 gene tend to convert glucose into lactate and preferentially use anaerobic glycolysis. (2) Lactate was accumulated when exposed to recurrent dehydration. (3) Lactic acid

stimulated the production of polyamine in macrophage. (4) Putrescine directly interacted with RTECs, upregulate CD2AP expression, promote its combination with PC2, and disrupt the stability of the PC1-PC2 complex on primary cilia of RTECs. (5) The dysfunction of primary cilia would finally cause initial cystogenesis.

Supplementary Files

This is a list of supplementary files associated with this preprint. Click to download.

- Supplementarymaterials.pdf
- Theprimersequences.docx